Time-resolved X-ray tomography of a fluidized bed

R.F. Mudde*
Kramers Laboratorium voor Fysische Technologie
Delft University of Technology
Pr.Bernhardlaan 6, 2628 BW Delft, The Netherlands.

September 15, 2008

Abstract

This paper discusses first results of bubbles moving through a fluidized bed imaged with an X-ray Tomographic Scanner. The scanner is made of 3 medical X-ray sources equipped with 30 $CdWO_4$ detectors each. The fluidized bed has a diameter of 23cm and is filled with Geldart B powder. The scanner measures the attenuation in a thin slice perpendicular to the column axis at a sampling frequency of 2500Hz.
The data collected during 2 seconds are reconstructed using the SART algorithm with a one-step-late correction. The reconstructions show the distribution of the bubbles in the 2-dimensional cross-section. By stacking these images, a 3-dimensional view of the bubbles in the column is represented.

Key words: X-ray tomography, time resolved, spatial resolution, SART, bubbling fluidized bed

1 Introduction

The simplest form of a fluidized bed is a cylinder containing a large quantity of small particles through which gas is flowing upwards. The gas velocity is such that the particles 'float' on the gas stream, creating a gas-particle mixture that has fluid like properties. Our understanding of fluidization is still far from complete, although during the last century computational methods have increased our knowledge significantly. However, due to their opaqueness, fluidized beds create serious problems for experimentalists. The well-known laser based techniques developed for single phase flows are inadequate for fluidized systems. Consequently, experiments on local phenomena are rare. However, solids are to some extend transparent to radiation such as X or γ rays and a variety of nuclear techniques have been developed during the last decade. In (Duduković 2000) the use of nuclear techniques in opaque multiphase systems is reviewed.
Radiation can be used to measure the volume fraction of gas (or equivalent of the solids) in a fluidized bed. If tomographic techniques are used, the volume fraction distribution in a cross section of the fluidized bed can be found. This is referred to as 'nuclear densitometry'. Several papers have appeared in literature, not only dealing with densitometry in fluidized beds, see e.g. (Kumar et al. 1995), (Kumar et al. 1997), (Kumar and Duduković 1997). For instance, (Shollenberger et al. 1997) measured the volume fraction in a 48cm-diameter bubble column, using a single beam-detector pair to perform horizontal, unidirectional scans over a cross-sectional plane assuming cylinder symmetry. (Mudde et al. 1999) followed a similar procedure to measure the solids

*e-mail: r.f.mudde@tudelft.nl

volume fraction in a turbulent fluidized bed. (Kumar et al. 1995) reported the use of a fan beam from a single γ source with multiple detectors. By rotating the source-detector combination around the column about 4000 projections could be taken, resulting in a spatial resolution of 5mm. As the total measuring time is about one hour, a time averaged volume fraction is obtained. This type of tomographic reconstruction is referred to as Computed Tomography or CT. In medical imaging, the use of X-ray tomography is standard practice. The source-detector system again rotates around the patient. This way high resolution, static images can be produced.

An alternative to the nuclear radiation is offered by electro-magnetic fields, like employed in Electrical Impedance Tomography. These EM-methods are fas, giving a high temporal resolution. images can be produced at rates of several hundreds per second(see e.g. (Reinecke and Mewes 1996), (Kühn et al. 1996), (Beck et al. 1998)). However, the EM-techniques work with so-called soft fields: a change in the electro-magnetic properties in one location changes the field everywhere in the domain. This makes reconstruction difficult and the resolution the center of the object is usually relatively poor. Nuclear densitometry relies on hard fields. Hence, they do not suffer from this problem. But, the nuclear techniques are rather slow. Due to inherent noise, the frame-rate (temporal resolution) that can be obtained is usually low.

A very fast X-ray tomographic system has been developed by Hampel and co-workers, see e.g. (Bieberle and Hampel 2006), (Bieberle et al. 2007). They generate the X-rays by moving an electron beam over a Tungsten element. They can create tomographic images up to a rate of 10,000 frames/s. This is evidently showing that nuclear techniques can also be fast.

In the present paper, we focus on the use of X-rays for tomographic imaging of bubbles in a 23cm fluidized bed. Our system consists of 3 X-ray sources that simultaneously radiate each a fan beam through the bubbling bed. The radiation is detected by 3*30 detectors. From the data collected, the solids distribution is reconstructed in the imaging plane. Consecutive images are stacked, giving an impression of the bubbles, their shape and spatial distribution. As far as we know, these are the first data of this kind.

2 Experimental Setup

The fluidized bed is formed by a 23cm inner-diameter tube (perspex, wall thickness 5mm) filled with 0.56mm sized polystyrene particles (st.dev. of particle size distribution is 0.16mm). The powder is of Geldart type B. The polystyrene has a density of $1.102 \cdot 10^3$kg/m^3. The mean density of loosely packed polystyrene particles is 625 kg/m^3. The minimum fluidization and minimum bubbling velocity are virtually identical for this powder: 0.12m/s. In the bubbling regime of fluidization, voids travel upwards through the powder mass. The ungassed height of the bed is 61cm. The air (room temperature) is via a wind box supplied to the bed through a porous plate (sintered bronze). A schematic of a fluidized bed with two bubbles in the measuring plane of the densitometer is given in fig.1.

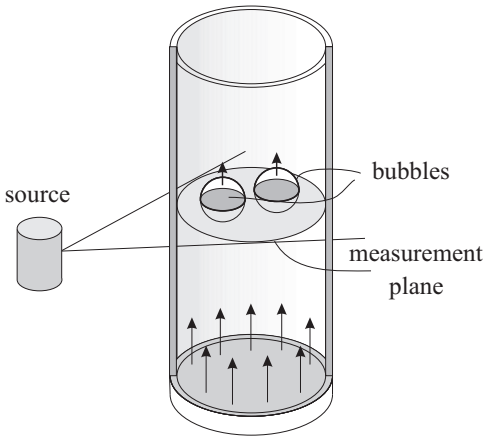

Figure 1: Fluidized bed with two bubbles in the measuring plane of the X-ray densitometer.

The X-ray sources are placed at 120° around the fluidized bed. Three arrays of sensors are placed opposite of the source. A photo of the scanner is shown in fig.(2). The distance from the X-ray-target to the center of the fluidized bed is 68.5cm, from X-ray target to the detectors is 138.6cm. The measuring plane is 50cm above the distributor plate.

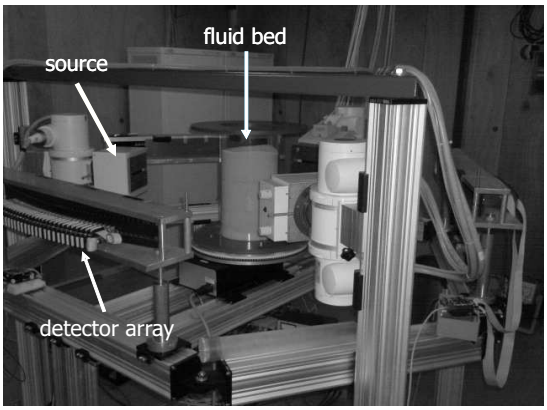

Figure 2: Photo of the tomographic X-ray scanner.

The X-ray source used is of standard medical type with a maximum X-ray energy of 150keV for source 1 and 133keV for the other two. We operate them at the lowest possible energy flux, which is in our case a tube current of 10mA. The detectors all consist of a $CdWO_4$ scintillation crystal optically coupled to a PIN photo diode. They are manufactured by Hamamatsu (type: S 1337 - 1010BR). Their crystal size is 10mm*10mm*10mm.
A curved plastic casing holds a horizontal array of 32 detectors. The curvature of the array is such that the distance to the focal point of the source is equal for all detectors. Of these detectors 30 are used to produce data for tomographic reconstruction, the two outermost detectors are used to monitor the alignment of the object vessel. The data are collected simultaneously at a sampling frequency of 2500Hz. The measured data are read out using a 12 bit ADC-card. Using thin copper plates (thickness varying from 1 to 3mm) in front of the detectors, the radiation incident on the detectors is reduce to a level that maximizes the dynamic range. Without this additional attenuation, detectors measuring rays traveling through the wall region would clip. Moreover, the same could happen to the other detectors if a very large bubble passes the measuring plane. The entire process is controlled via a workstation that send out the trigger signals to the sources and reads out the detectors.

3 Tomographic Reconstruction

3.1 Measuring Principle & Calibration

Each detector measures the attenuation of the X-rays in a thin cone. In the reconstruction this is treated as a thin line. If such a line if mono-energetic γ- or X-rays is transmitted through a closed system containing a particle-gas two-phase mixture, the number of photons registered per second, R, follows from the Lambert-Beer law:

$$R = R_0 exp\left[-\left((1-\alpha)\mu_p + \alpha\mu_g\right) d\right] \quad (1)$$

where R_0 is the number of photons registered per second when the system is in vacuum; μ_p and μ_g denote the linear absorption coefficient of the particle and gas phase; α is the volume fraction of the gas phase; d is the inner diameter of the system. It should be noted that the attenuation characteristics of the fluidized bed wall is incorporated in R_0. Both μ_p and μ_g are functions of the photon energy E. An X-ray source generates a wide spectrum of photon energies. In order to deal with this, we have calibrated all detector individually by placing various amounts of packed powder in between a source and its detectors. This way a calibration curve is made, of the form $A_{cal} + B_{cal} \cdot exp\left(-x/C_{cal}\right)$, with x the distance traveled by the beam through the powder phase. Using this calibration, the data measured

in an experiment can be converted to a measured distance, x_{meas}, the beam travels through the powder mass.

Tomographic Reconstruction
Various reconstruction techniques exist. For instance, the Filtered Back Projection algorithm can be used. A second class is formed by the algebraic techniques, which are iterative and reconstruct the object function on a discretized domain. Although significantly slower, algebraic methods offer more flexibility in terms of limited data sets and are more appropriate for the CT configuration system under consideration here. Detailed accounts of reconstruction techniques can be found in (Brooks and DiChiro 1976), (Herman 1980) or (Kak and Slaney 1988).

We would like to reconstruct the gas fraction, or equivalently the solids fraction as they add up to one. We use the calibration curve to convert the measured line-averaged attenuation into a line averaged solids fraction. We will reconstruct the solids fraction $\alpha(x, y)$ in a pixel representation of the cross-section of the fluidized bed. The number of pixels is an independent parameter that we can select. A good value for our case is a square pixel array of 65*65 pixels. The circle representing the cross-section of the fluidized bed exactly fits in this square. All pixels outside the circle have a solids fraction of zero. For a given ray, traveling through the object, the total solids fraction on the line, p_i, referred to as *ray sum*, can be estimated as

$$\tilde{p}_i = \sum_{k=1}^{N} W_{ik}\alpha_k \qquad (2)$$

with α_k the pixel-based value of the solids fraction distribution and W_{ik} the weighing factor for pixel k for the i^{th} ray through the object. We use a linear weighing matrix W. Hence, the weighing factor W_{ik} is the length of ray i through pixel k (see fig.(3)).

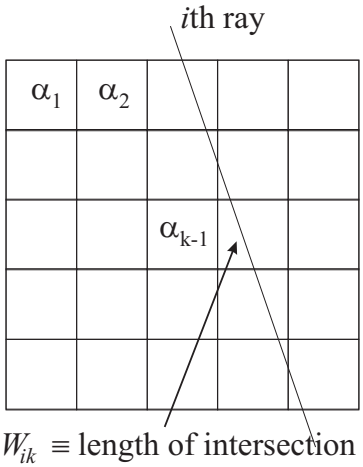

Figure 3: coordinate system

To reconstruct the image we need to solve the unknown pixel-averaged solids fraction α_k from eq.(2) for M different rays on N pixels. As the number of independent measurements is only 3*30=90 and the number of unknown pixels is easily 1000 or more, the problem is ill-posed. Moreover, there will be measuring noise in the data. We write formally:

$$\vec{p} = \mathbf{W} \cdot \vec{\alpha} + \vec{\epsilon} \qquad (3)$$

where $\vec{\epsilon}$ contains all errors. The Algebraic Reconstruction Techniques (ART, see e.g. (Brooks and DiChiro 1976)) are designed to minimize the mismatch between the data $\vec{p}$ and $\mathbf{W} \cdot \vec{\alpha}$. They are iterative methods that solves $\vec{p} = \mathbf{W} \cdot \vec{\alpha}$. We use the Simultaneous Algebraic Reconstruction Technique (SART) (Andersen and Kak 1984). Instead of sequentially updating the pixels on a ray-by-ray basis, SART simultaneously applies to a pixel the average of the corrections generated by all rays. This offers a reduction in the amplitude of the salt and pepper noise that is usually present in ART. However, it goes at the expense the computation time. The SART algorithm is given by:

$$\alpha_k^{n+1} = \alpha_k^n + \frac{w}{W_{+,k}} \frac{p_i - \tilde{p}_i}{W_{i,+}} W_{ik} \qquad (4)$$

with $W_{+,k} = \sum_{i=1}^{N} W_{ik}$, $W_{i,+} = \sum_{k=1}^{N} W_{ik}$ and w a relaxation parameter that should be between $\{0,2\}$; we have set it to 1. Originally, SART is part of the ART family. However, recently (Jiang and Wang 2003) have shown that SART is a maximum likelihood estimator for the mapping of α in case the error in eq.(3) is purely stochastic with a Gaussian distribution.

Still, pepper and salt noise will be present in the images. This can be reduced by using a so-called one-step-late algorithm (see (Green 1990)). We invoked an algorithm based on the median root function (suggested first by (Alenius and Ruotsalainen 1997)). It effectively removes pepper and salt noise, but keeps the edges of larger objects sharp enough. In the reconstruction algorithm an extra step is added to eq.(4):

$$\alpha_{OSL,k}^{n+1} = \frac{1}{1 + \beta \dfrac{\alpha_{OSL,k}^{n} - Med(\alpha_{OSL,k}^{n})}{Med(\alpha_{OSL,k}^{n})}} \alpha_{k}^{n+1} \tag{5}$$

with α_k^n the value of pixel k after the nth SART step and $\alpha_{OSL,k}^n$ the same after the nth one-step-late correction.

The median filter $Med(\alpha_k)$ sets the value of the kth pixel equal to the median of the pixel values contained in the kth pixel neighborhood. The definition of this pixel neighborhood is the only parameter of the median filter. We use a 3×3 neighborhood; a 5×5 neighborhood causes too much smearing. The parameter β in eq.(5) again controls the weight of the correction.

4 Experimental Results

4.1 Calibration

All detectors are individually calibrated. For each calibration point a known amount of packed solid particles is placed inside the fluidized bed. This includes a completely empty and a completely filled bed. Seven different points are measured this way. The X-ray sources are switched on for one second and the data collected are averaged. An exponential curve is fitted through the averaged data points. An example of a calibration curve and the corresponding data is given in fig.(4).

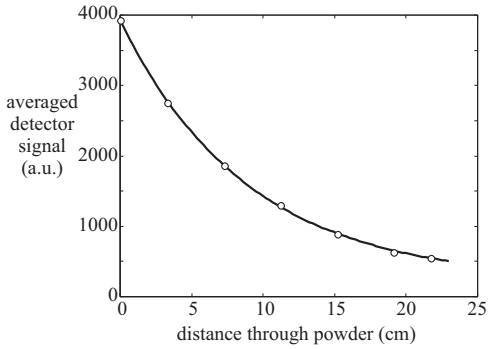

Figure 4: Calibration curve of one of the detectors with its corresponding beam going almost through the bed center

4.2 Pre-processing of tomographic data

The X-ray sources all three suffer from a ripple on their high-voltage supply. This shows up in the measured data as a saw tooth behavior of the data in time. The frequency of this saw tooth depends on the source: for source one it is about 400Hz, for the other two around 90Hz. In principle, the data can be corrected for this fluctuation in source strength, e.g. by using the two outer detectors of each detector array. They measure outside the fluidized bed and thus directly see the fluctuations of their source. In the present work, we have averaged the data first over one period of the 28 data points and moved in steps of 10 time steps through the data series for each new reconstruction. This obviously reduces the time resolution of the images from 2500 frames per second to about 100 frames per second. This is, however, not a principle reduction of the time resolution of the tomographic scanner, but for the moment a practical solution. The averaged data are than, using the calibration

curves, in a few steps converted to a line-averaged solids fraction as measured by a detector. Note that the thickness of the perspex walls of the vessel is via the calibration removed from the data.

4.3 Results

A fluidization experiment is run in the bubbling regime. Experiments are run at a superficial gas velocity of 1.3 and 1.6 times U_{mf}. data are taken for a period of 2 seconds. This generates potentially 5000 images. However, due to the pre-processing, only 500 images are reconstructed that are not fully independent. The number of independent images is 180. In fig.(5) the response of one of the detectors is shown. The corresponding path for the X-rays is almost through the center of the bed. Clearly, the passage of bubbles is recorded. The base line has the same value as the minimum fluidized bed case.

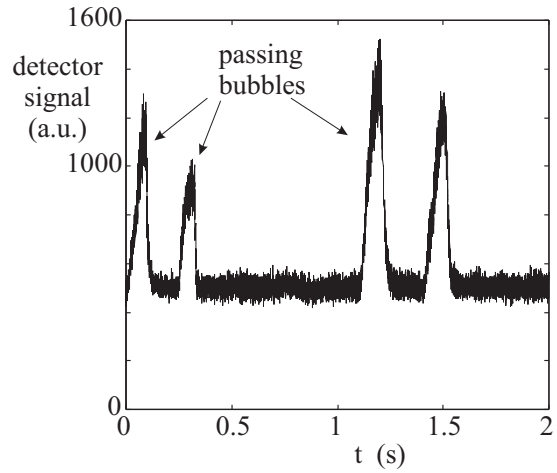

Figure 5: Raw signal of one of the detectors ($U_{sup} = 1.3U_{mf}$
. The corresponding X-rays travel almost through the center of the bed.

The raw signals are pre-processed as described above and fed to the reconstruction algorithm. Each reconstruction starts from an initial guess: a uniform fluidized bed with no bubbles. On a reconstruction grid of 65*65 pixels, a single image reconstruction takes about 7 seconds of computer time (programs are written in FORTRAN and run on a single PC with processor speed of 1.2GHz). Figure (6) shows an image cutting through a bubble with a diameter of about 8cm. This image is a filtered version of the corresponding raw image. A Gaussian filter (the filter kernel is based on a 3*3 pixel representation) is used for this.

Figure 6: Image showing the passage of a bubble.

In the figure, a 'tail' can be observed going from the bubble towards the upper right corner of the figure. This is an artifact of the reconstructions and most likely caused by the use of only three sources. From simulations (Mudde et al. 2005) we found, that a 5 source system suffers less from this effect. This artificial tail is taken out by thresholding the images: all pixel values below 125 are set to zero. The images have gray values ranging from 0 (black) to 255 (white).
The present set-up does not allow for velocity measurements. That can be relatively easy made by stacking a second ring of detectors above the present ones. This way a second measuring plane is formed and velocity measurements are possible. The two planes will not be exactly parallel,

but slightly diverse making the interpretation less straight forward. This is a step for future work. Here, we have estimated the velocity of the bubbles to be about 50cm/s (a single bubble with an equivalent diameter of 6cm has a rise velocity of this magnitude according to the Davidson relation $v_b = 0.71\sqrt{gd_{eq}}$ with g the acceleration of gravity and d_{eq} the equivalent diameter of the spherical-cap shaped bubble). The time interval between two consecutive images we have reconstructed is 1/250s. The bubble shown in fig.(6) is visible in 20 images, corresponding to a time interval of 80ms. Combined with the estimated velocity, we conclude that the bubble is 4cm in height. We have stacked the images giving a quasi 3-dimensional picture of the flow in the column. The scaling is chosen such that the bubble of fig.(6) are about 4cm high. This is shown in fig.(7)

Figure 7: Stacked image showing four bubble. The dotted lines represent the column of the bed. Superficial velocity $\approx 1.3U_{mf}$.

The bubbles are clearly visible: they are of the spherical cap type with flat bottoms. One smaller bubble, most to the right) is moving along the column wall. The entire figure is 168 images, which is equivalent to 0.67s.

A similar experiment is run at $1.6U_{mf}$. Again 2 seconds of data are recorded and reconstructed. The bubbles captured are shown in fig.(8). As expected, the bubbles are larger. The vertical trace of gray pixels is an artifact of the reconstruction and probably caused by noise.

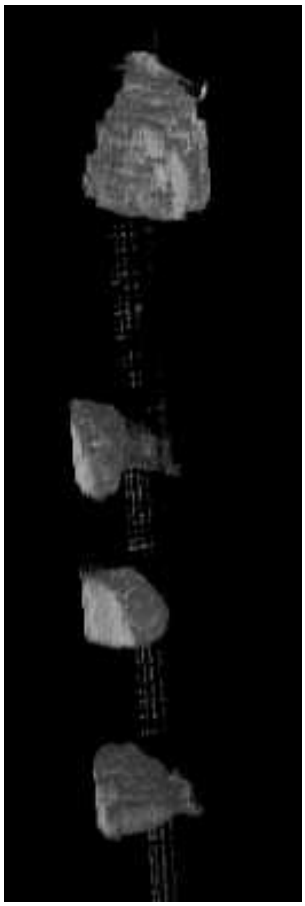

Figure 8: Stacked image showing four bubble. The three lower bubble move along the column wall. Superficial velocity $\approx 1.6U_{mf}$.

Concluding Remarks

In this paper, we present first results of the bubbles in a fluidized bed made with an X-ray based tomographic scanner. The scanner consists of three standard medical X-ray tubes with 30 detectors containing $CdWO_4$ scintillator crystals. The data are collected at a frequency of 2500Hz. Due to a voltage ripple in the sources the full speed can not be used. Therefor the data are averaged over 28 images and every 10 images a new average is calculated. Thus, the effective frequency of the results presented is 250Hz. This, however, not a principle limitation.
We have reconstructed the images on a 65*65 grid with a pixel size of 3.5mm. the bed diameter is 23cm and clearly spherical cap like bubbles are found. We conclude that an X-ray based tomographic scanner has lots of potential to investigate the motion of bubbles ion a fluidized bed in a tomographic way.

References

Alenius, S. and U. Ruotsalainen (1997). Bayesian image reconstruction for emmission tomography based on median root prior. *Eur. J. of Nucl. Med. 22*.

Andersen, A. H. and A. C. Kak (1984). Simultaneous algebraic reconstruction technique (sart): a superior implementation of the art algorithm. *Ultrasonic Imaging 6*, 81–94.

Beck, M. S., T. Dyakowski, and R. A. Williams (1998). Process tomography - the state of the art. *Trans. Inst. Meas. and Control 20(4)*, 163–177.

Bieberle, M., F. Fischer, E. Schleicher, U. Hampel, D. Koch, K. Aktay, H.-J. Menz, and H.-G. Mayer (2007). Ultrafast limited-angle-type x-ray tomography. *Appl. Phys. Lett. 91*, 123516/1–123516/3.

Bieberle, M. and U. Hampel (2006). Evaluation of a limited angle scanned electron beam x-ray ct approach for two-phase pipe flows. *Meas. Sci. Technol. 17*, 2057–2065.

Brooks, R. A. and G. DiChiro (1976). Principles of computer assisted tomography (cat) in radiographic and radioscopic imaging. *Phys. Med. Biol. 21*, 689.

Duduković, M. P. (2000). Opaque multiphase reactor: Experimentation, modeling and troubleshooting. *Oil & Gas Sci. and Techn. - Rev. IFP 55*, 135.

Green, P. J. (1990). Bayesian reconstruction from emmission tomography data using a modified em algorithm. *IEEE Trans. on Med. Imag. 9*, 84–93.

Herman, G. T. (1980). *Image reconstruction from projections - the fundamentals of computerized tomography*. Academic Press.

Jiang, M. and G. Wang (2003). Convergence of the simultaneous algebraic reconstruction technique (sart). *IEEE Trans. on Image Proc. 12*, 957–961.

Kak, M. and M. Slaney (1988). *Principles of computerized tomographic imaging*. New York: IEEE Press.

Kühn, F. T., J. C. Schouten, R. F. Mudde, C. M. Van den Bleek, and B. Scarlett (1996). Analysis of chaos in fluidization using electrical capacitance tomography. *Meas. Sci. & Techn. 7*, 361.

Kumar, S., D. Moslemian, and M. Duduković (1995). A gamma ray tomographic scanner for imaging void fraction distribution in bubble columns. *Flow. Meas. Instr. 6*, 61.

Kumar, S., D. Moslemian, and M. Duduković (1997). Gas holdup measurments in bubble columns using computed tomography. *AIChE J. 43*, 1414.

Kumar, S. B. and M. P. Duduković (1997). *Computer assisted gamma and X-ray tomography: applications to multiphase flow*

systems, In: *Non-invasive Monitoring of Multiphase Flows, Chaouki, J. and Larachi, F. and Duduković, M.P. (eds.), Ch.2.*, pp. 43–103. Elsevier.

Mudde, R. F., P. R. P. Bruneau, and T. H. J. J. Van der Hagen (2005). Time-resolved gamma-densitometry imaging within fluidized beds. *Ind. & Eng. Chem. Res. 44*, 6181–6187.

Mudde, R. F., W. K. Harteveld, H. E. A. Van den Akker, T. H. J. J. Van der Hagen, and H. Van Dam (1999). Gamma radiation densitometry for studying the dynamics of fluidized beds. *Chem. Eng. Sci. 54*, 2047.

Reinecke, N. and D. Mewes (1996). Recent developments and industrial research applications of capacitance tomography. *Meas. Sci. & Techn. 7*, 233.

Shollenberger, K. A., J. R. Torczynski, D. R. Adkins, T. J. O'Hern, and N. B. Jackson (1997). Gamma-densitometry tomography of gas holdup spatial distribution in industrial-scale bubble columns. *Chem. Eng. Sci. 52*, 2037.